

Controlled Deposition, Soft Landing, and Glass Formation in Nanocluster-Surface Collisions

Hai-Ping Cheng and Uzi Landman

Molecular dynamics simulations have been used to investigate the dynamics and redistribution of energy during the impact of a nanocrystal with adsorbed liquid films. Although impact of a 32-molecule NaCl cluster on a solid surface at 3 kilometers per second leads to melting, disordering, fragmentation, and rebounding, the same size cluster colliding with a liquid neon film transfers its energy efficiently to the liquid for a controlled soft landing. Impact on a higher density film (argon) leads to rapid attenuation of the cluster velocity, accompanied by fast heating. Subsequent disordering, melting, and fast cooling by evaporation of argon quench the cluster to a glassy state. These results suggest a method for the controlled growth of nanophase materials.

The growth and evolution of the shapes and forms of materials are commonly observed as the assembly of small elementary units (atoms or molecules, small clusters, nanoscale aggregates, or larger particles) (1–4). Much of the research into material growth is focused on the fundamental physical and chemical behavior of these units and their aggregation processes, such as kinetics and dynamics of nucleation, properties of fluid-solid interfaces, phase transformations, collision dynamics, and energy transfer (5). Identification of the parameters that control growth—for example, the nature of the deposited particles, the deposition rates, and substrate conditions—and their application in materials preparation techniques are of great basic and technological significance. Moreover, correlations between physical and chemical properties and their ultrafine microstructure are abundant among natural and fabricated materials.

Research efforts have begun to focus on methods of preparation and investigation of nanophase or nanostructured materials—that is, solids composed of nanoscale structural units that maintain their individual characteristics after consolidation. The interest in such materials arises from the electronic, optical, magnetic, mechanical, and chemical properties they may exhibit (3).

We report on theoretical investigations of the energetics of collisions of crystalline nanoclusters impinging on fluid films adsorbed on solid surfaces (6–8). Our results reveal the nature of the energy conversion and redistribution, crater formation, heating, melting, cooling, and shock generation that occur when a nanocrystal collides with a fluid surface at hypervelocities. Furthermore, we find that the collision process and final state of the system can be controlled by an appropriate choice of the liquid film for a given cluster.

To investigate the atomic-scale dynam-

ical mechanisms of energy conversion in collisions of a vibrationally cold (NaCl)₃₂ cluster with a bare (001) NaCl surface and with adsorbed fluid neon or argon films, chosen because of their chemically inert nature, we have used molecular dynamics (MD) simulations, in which the Newtonian equations of motion of a system of interacting particles are integrated by a computer. The calculational cell of the crystalline NaCl surface consisted of n_d layers of dynamic particles ($n_d = 5$ for the adsorbed neon film, $n_d = 4$ for argon) with 400 particles per layer, arranged in a rock salt crystalline structure that exposed the (001) surface. These layers were positioned on top of four layers of a static NaCl crystal of the same crystallographic orientation. For simulations involving adsorbed films, the system was prepared with a fluid film equilibrated on top of the crystalline surface. The substrate calculational cell was repeated periodically in the two directions parallel to the (001) surface plane with no boundary conditions applied in the normal (z) direction. For NaCl clusters, the lowest energy structures consist of approximate cubes or rectangular parallelepipeds (9) with alternating Na⁺ and Cl⁻ ions. In our simulations, we chose a 64-ion cubic cluster, (NaCl)₃₂, initially equilibrated at 50 K.

The intra- and inter-ionic pairwise interactions in the substrate and in the nanocluster were described by potentials that included Coulomb and Born-Mayer repulsion terms, which provide an appropriate description of bulk NaCl (10). The interactions between the rare gas atoms were described by pairwise 6-12 Lennard-Jones potentials (11) with well-depth parameters $\epsilon_{Ar} = 0.01028$ eV and $\epsilon_{Ne} = 0.00405$ eV and length parameters $\sigma_{Ar} = 6.435 a_0$ and $\sigma_{Ne} = 5.140 a_0$ (where $a_0 = 0.529 \text{ \AA}$ is the Bohr radius). The interactions between the rare gas atoms and the Na⁺ and Cl⁻ ions were described by the potentials developed by Ahlrichs *et al.* (12).

The target surfaces (the NaCl surface,

bare or with an adsorbed thin film of argon or neon) were initially equilibrated at 300, 95, and 40 K, respectively. During subsequent simulations, the temperature was controlled by the application of stochastic thermalization (13), at the appropriate temperature, to the bottom dynamic layer of the solid surface region with a stochastic collision frequency of $7.75 \times 10^{-3} \text{ fs}^{-1}$. The equations of motion were integrated with the use of the fifth-order Gear algorithm (14) with a time step $\Delta t = 0.25 \text{ fs}$, which assures conservation of energy throughout the collision process.

After equilibration of the separated collision partners, a velocity of 3 km s^{-1} (that is, a kinetic energy of 2.72 eV per NaCl molecule) was assigned to the cluster ions in the direction of incidence normal to the surface, and the collision process was simulated. In discussion of the energetics of the cluster, it is instructive to distinguish a kinetic energy component representing overall (center of mass) motion (K_c^{cm}) from an internal kinetic energy (K_c^{int}) component corresponding to particle “thermal” motion. We take K_c^{int} to be the kinetic energy in a coordinate system that is moving with the cluster’s center of mass. In equilibrium steady-state conditions, equipartition of energy between the various degrees of freedom results in a direct relation between the internal temperature, T , of a set of N particles and the average of K_N^{int} ($3Nk_B T/2 = \langle K_N^{int} \rangle$, where k_B is the Boltzmann constant). Although we do not expect that full equilibrium will be achieved throughout most of the collision processes, we often express the internal kinetic energy of a set of particles as their kinetic temperature.

Upon collision of the incident cluster with the target surface, attenuation of its incident translational motion is accomplished by the conversion of the cluster incident kinetic energy (K_c^{cm}) (Fig. 1A) into potential and kinetic energies of internal degrees of freedom of the cluster (K_c^{int} and $E_{p,c}^{int}$) and those of the substrate.

The dependence of the attenuation rate on the substance of the target film is reflected also in the penetration depth and dynamics of dissipative processes. Interestingly, in the case of the higher density film (Ar), the translational energy of the cluster is lost in the immediate vicinity of the liquid surface (depth of $\sim 4 \text{ \AA}$), whereas a more gradual energy conversion for a lower density film (Ne) occurs over a larger distance range ($\sim 10 \text{ \AA}$) (Fig. 1B).

The variation in time of the total internal energy of the cluster, relative to its initial translational energy, is different for the three collision processes (Fig. 2A). The results demonstrate that the rate of energy deposition into the cluster and the branching ratio between ΔE_c^{int} and the energy dissipated into the fluid substrate depend

School of Physics, Georgia Institute of Technology, Atlanta, GA 30332.

strongly on the nature of the target surface. Overall, the internal energy increase of the cluster incident on the Ar film is about twice that for collision with the Ne film. The magnitude of the initial ($t \leq 2$ ps) increase of the total internal energy of the cluster colliding with the Ar film is similar to that for incidence on a bare, solid NaCl surface; the Ar film behaves like a "hard mattress."

We can estimate the energy deposited into a fast, colliding, nonrigid cluster during attenuation of its incident velocity (15) by considering the work of deformation done on the impinging cluster by the target fluid, yielding the branching ratio

$$\Delta E_c^{\text{int}}/K_c^{\text{cm}}(0) \propto \left[\frac{\rho_l c_l}{\rho_s c_s} \right]^2$$

where ρ_l and c_l are the density and sound velocity, respectively, for the liquid, and ρ_s and c_s are the corresponding parameters for the solid cluster (equivalent expressions in terms of liquid and solid densities and compressibilities, or elastic moduli, can be easily obtained). The above expression portrays the collective (condensed phase) nature of energy transfer and redistribution in our system (15).

The partitioning of the energy deposited

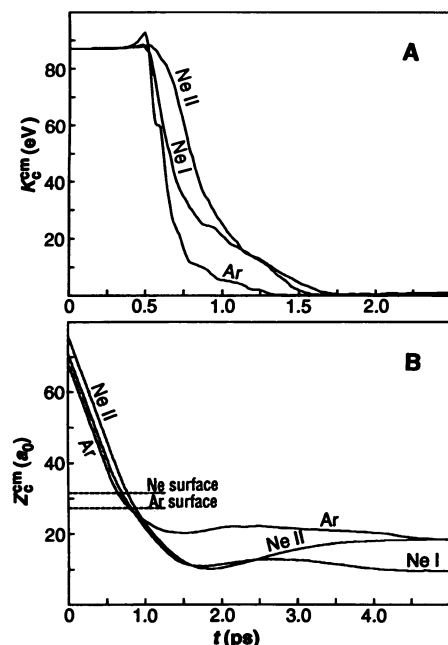


Fig. 1. (A) Kinetic energy and (B) center-of-mass position (on z axis) of a $(\text{NaCl})_{32}$ nanocluster incident on adsorbed liquid Ar or Ne films plotted versus time. For the Ne film, two initial orientations, Ne I and Ne II, correspond to cubic clusters impinging with the face or corner of the cube, respectively, directed toward the target surface. The origin of the distance axis in (B) is at the average location of atoms in the topmost layer of the underlying crystalline NaCl substrate. The average locations of the top of the liquid films are indicated.

into the cluster between the potential (Fig. 2B) and kinetic components (shown as the internal kinetic temperature, T_c^{int}) (Fig. 2C) is reflected also in the state of the cluster subsequent to the collision with the surface. The large magnitudes of $\Delta E_{\text{p,c}}^{\text{int}}$ and T_c^{int} for collision with the Ar film lead to melting and disordering of the cluster, while maintaining its compositional integrity (Fig. 3, A and B). On the other hand, the smaller values accompanying deposition into the lower density Ne film are associated with processes that preserve the overall shape and crystalline order of the cluster (Fig. 3, C and D).

The interruption of the incident cluster motion at the target surface results in heating, structural deformations, possible fragmentation (for incidence on a bare crystalline surface), splash evaporation of film atoms, the development of shock conditions, and the eventual dissipation of energy in the underlying crystalline substrate. Incidence into the higher density

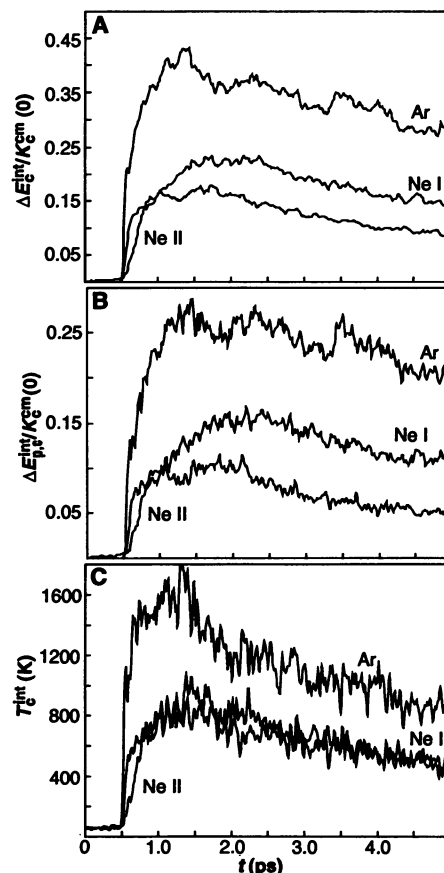


Fig. 2. Time evolution of the changes in (A) total internal energy and (B) internal potential energy from the average initial values for a $(\text{NaCl})_{32}$ cluster colliding with liquid Ar or Ne films (Ne I and Ne II as in Fig. 1), plotted relative to the initial total incident translational energy of the cluster [$K_c^{\text{cm}}(0) = 87$ eV]. (C) The corresponding variations with time of the internal kinetic temperature of the cluster.

fluid (Ar) (Fig. 2C) leads to ultrafast heating of the cluster ($\sim 5 \times 10^{15} \text{ K s}^{-1}$) to a maximum temperature $T_c^{\text{int}} \sim 1600$ K (a ~ 30 -fold increase from the initial vibrational temperature of the cluster). At this stage ($t < 1.55$ ps), the cluster is superheated, maintaining a high degree of structural order.

Subsequent cooling of the cluster occurs first at a fast rate ($\sim 0.5 \times 10^{15} \text{ K s}^{-1}$, from 1600 to 1200 K in the interval $1.55 \text{ ps} \leq t \leq 2.5$ ps), mainly through the disordering and effective melting of the cluster, with some evaporation of Ar atoms and heat dissipation through the liquid. During this fast cooling stage, the thermally shocked, melted cluster is quenched to a highly disordered glassy structure, confined and

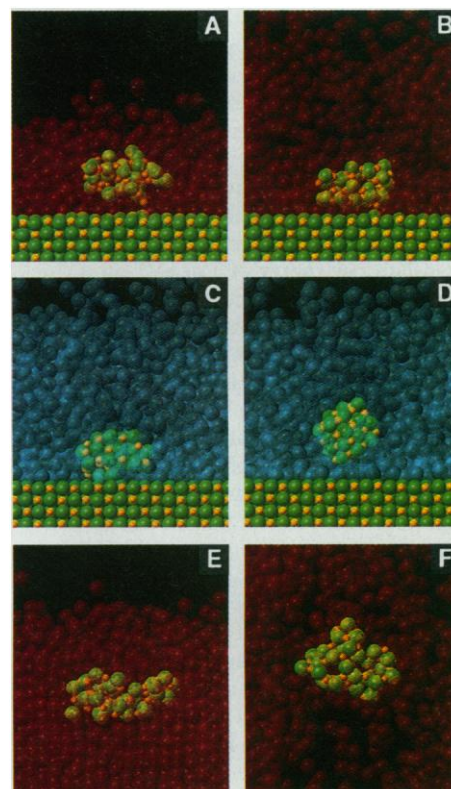


Fig. 3. Selected atomic configurations from simulations of collisions of an initially ordered NaCl nanocrystal (Na, yellow; Cl, green) with adsorbed Ar (red) and Ne (blue) fluids. Disordered (glassy) $(\text{NaCl})_{32}$ cluster at (A) $t = 2$ ps and (B) $t = 8$ ps in collision with an Ar film. Ordered clusters, from the limiting cases of initial orientation (C) Ne I and (D) Ne II, soft landed on a Ne film ($t = 5$ ps). The structural defect in (C) was caused by the initial impact with the liquid surface. Glassy nanocluster configurations, at (E) $t = 2$ ps and (F) $t = 22$ ps, formed in a higher energy collision (center-of-mass velocity of 4 km s^{-1}) with a thick Ar film (only a portion of the system surrounding the cluster is shown). Note the "porous" structure of the fluid in (F). In all cases, the structures of the clusters at longer times remain virtually the same as the ones shown.

frustrated by the presence and partial incorporation of Ar atoms (Fig. 3A). The subsequent cooling stage ($t \geq 2.5$ ps) is characterized by a slower rate ($\sim 10^{14}$ K s^{-1}) that is dominated by evaporative and heat-transport processes (although results are shown in Fig. 2 for $t \leq 5$ ps, simulations continued for longer times, and temperature continued to decrease with time). As the process continues, the disordered cluster approaches the underlying crystalline substrate, where it is eventually deposited (Fig. 3B).

Throughout the evolution of the system, the cluster remains in a highly disordered state, characterized by a significant excess internal potential energy above that corresponding to the fully ordered ground state of the cluster. The initial sudden jump to high temperature coupled with the ultrafast cooling arrest the cluster in a configurationally disordered state, preventing activated reordering and structural annealing of the cluster (16).

To further investigate the consequences of collisions with an Ar surface, we performed simulations involving a $(\text{NaCl})_{32}$ cluster incident with high velocity (4 km s^{-1} , which corresponds to a total cluster translational energy of 154 eV) on a thick Ar film (~ 60 Å). In this system, the cluster penetrates deeper into the liquid before stopping (~ 15 Å). In the first stage ($t \leq 3$ ps) following the initial ultrafast temperature jump (to $T_c^{\text{int}} \sim 2500$ K), the superheated cluster melts and then cools into a glassy state with high internal potential energy at a quench rate of $\sim 0.75 \times 10^{15}$ K s^{-1} (Fig. 3E).

Subsequent cooling to ~ 600 K in the interval $3 \text{ ps} \leq t \leq 8 \text{ ps}$ occurs mainly through heat transport in the hot liquid at a rate of $\sim 10^{14}$ K s^{-1} . During this stage, the cluster becomes buoyant, driven upward by the pressure gradient and refractory waves developed in the liquid. Further cooling ($t \geq 8$ ps), at a rate of $\sim 10^{13}$ K s^{-1} , is assisted by evaporation of the liquid and the continued transport of heat to the cold solid substrate. Throughout the process, the cluster remains arrested in a configurational glassy state (Fig. 3F) characterized by an internal potential energy $\sim 20\%$ higher than that of the disordered clusters obtained by means of lower energy incidence, as discussed above. These results illustrate that variation of the initial impact energy of the cluster allows access to various local minima of the multidimensional configurational and potential surface comprising the ensemble of glassy states of the cluster.

Collision of the cluster with a Ne liquid surface, which is characterized by a relatively smaller energy flow into the cluster than that for the Ar film (Fig. 2A), leads also to fast heating (though at one-third the rate

for the Ar film) to a maximum temperature of ~ 800 K, occurring over a comparatively longer attenuation length (Fig. 1B). Under these conditions, the heated cluster, embedded in the hot Ne liquid, does not undergo melting, maintaining to a large degree its original crystalline order and

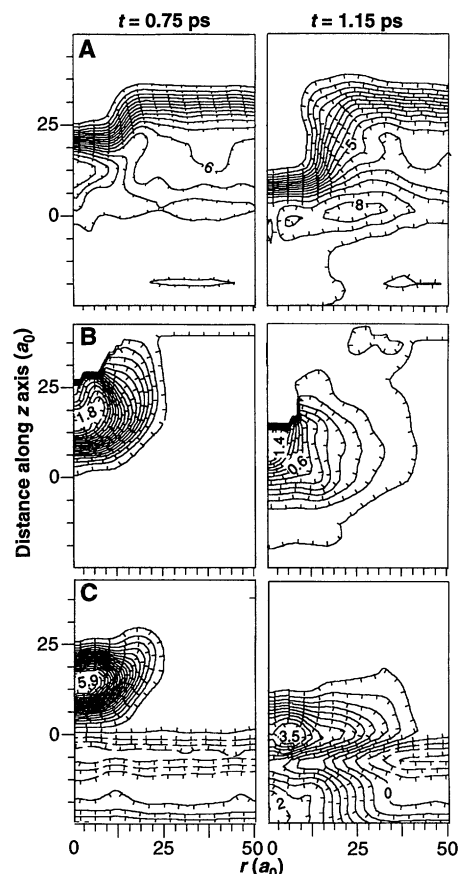


Fig. 4. Contours of (A) density (ρ), (B) temperature (T), and (C) pressure (P) of the target surface (initially at $T = 40$ K) recorded at $t = 0.75$ ps (left column) and $t = 1.15$ ps (right column) during the deposition of a $(\text{NaCl})_{32}$ nanocrystal (Ne I orientation) on a Ne film adsorbed on a NaCl crystal. The origin of the z axis (normal to surface) is at the average location of the topmost layer of the crystalline NaCl substrate. The average thickness of the film is $31 a_0$. In the calculation of the contours of a property at any given region, the value was weighted by a Gaussian of width $3a_0$ (δ). Tick marks on contour lines point in the direction of increase in the value. The increment between neighboring contours is $\Delta_\rho = 5 \times 10^{-4} a_0^{-3}$, $\Delta_T = 94$ K, and $\Delta_P = 0.29$ GPa, and the indicated values associated with selected contours are in units of $10^{-3} a_0^{-3}$, 10^3 K, and gigapascals for ρ , T , and P , respectively. Note the formation of a crater in the fluid caused by the incoming cluster. Fluid particles propagate down toward the solid substrate and sideways in the film, leading to densification and bulging of the fluid (A). The pressure and temperature impulses propagate down and expand radially, transmitting at the latter time into the underlying solid substrate (B and C).

shape. During subsequent evolution of the system, cooling occurs through massive evaporation of the liquid and dissipation to the substrate. Eventually, the deposited cluster “soft lands” on the crystalline surface (Fig. 3, C and D). Here, as well as in the other cases, most of the excess gas atoms may be desorbed by heating of the substrate at the end of the process without substantial alteration of the state of the deposited nanocluster.

Impact of the incident cluster causes a strong perturbation in the target liquid film. Density contours of a Ne film (Fig. 4A) illustrate crater formation in the liquid in the region occupied by the incident cluster, which is accompanied by densification of the liquid (up to 30% above normal) under the impact zone and sideways flow and bulging of the displaced liquid that surrounds the penetrating cluster. The displacement of the liquid and the deposition of energy into it by the colliding cluster generate shock conditions, as seen in the temperature (Fig. 4B) and pressure (Fig. 4C) distributions. From these results, we observe that the collision generates high density, temperature (up to 1800 K), and pressure (up to ~ 6 GPa) shock impulses in the liquid, emanating from the contact zone, propagating down into the underlying solid, and expanding sideways in the film. These processes lead to the rapid dissipation of the deposited impact energy, partly through the supporting solid surface and partly through the displacement and bulging of the film and the eventual evaporation of liquid particles.

These results suggest a method for the controlled growth of nanophase materials based on epitaxial deposition of clusters, prepared and selected according to mass while in the gas phase, onto adsorbed liquid films. In addition, the method could allow the controlled preparation of well-characterized samples for investigations of supported clusters with the use of tip-based (scanning tunneling and atomic force) microscopes. As shown above, the nature of the deposited nanoscale growth units (shape, as well as crystalline versus glassy structure) may be controlled for a given incident cluster by means of the appropriate selection of the target liquid film (select collision partners with appropriate mass density and elastic moduli ratios) and incident translational energy of the clusters. Although we investigated the deposition of an ionic cluster on rare gas fluid targets, we expect that our conclusions apply to other materials (such as metal and semiconductor clusters and other fluid surfaces). In particular, polyatomic fluids may prove useful as substrates because excitations of internal vibrations, in addition to translational degrees of freedom, may provide efficient energy transfer channels.

Finally, the ultrafast heating and cooling rates (in excess of 10^{14} K s⁻¹) of finite aggregates that may be achieved by high-velocity collisions of clusters with liquids exceed the record laboratory rates reported to date (17, 18). Consequently, the methods suggested here may open new experimental avenues for ultrafast heat processing and for the preparation and exploration of nanoglass materials aggregates.

REFERENCES AND NOTES

1. R. Ludeke and K. Rose, Eds., *Interfaces and Contacts* (North-Holland, Amsterdam, 1983); P. S. Ho and K. N. Tu, Eds., *Thin Films and Interfaces* (North-Holland, Amsterdam, 1982); J. W. Matthews, Ed., *Epitaxial Growth* (Academic Press, New York, 1975); see reviews in *Mater. Res. Bull.* **13**, 18 (1988).
2. I. Yamada, G. H. Takoska, H. Usui, T. Takagi, *J. Vac. Sci. Technol.* **A4**, 722 (1986); I. Yamada, *Appl. Surf. Sci.* **43**, 23 (1989); T. Takagi, *Ionized-Cluster Beam Deposition and Epitaxy* (Noyes, Park Ridge, NJ, 1988); H. Haberland, M. Karrais, M. Mall, *Z. Phys. D* **20**, 413 (1991); J. H. Weaver and G. D. Waddill, *Science* **251**, 1444 (1991).
3. See review by H. Gleiter, *Nanostruct. Mater.* **1**, 1 (1992), and references therein.
4. J. C. Brice, *The Growth of Crystals from Liquids* (North-Holland, Amsterdam, 1973); for molecular dynamics simulations of liquid-phase epitaxy, see U. Landman, C. L. Cleveland, C. S. Brown, *Phys. Rev. Lett.* **45**, 2032 (1980); U. Landman, W. D. Luedtke, M. W. Ribarsky, R. N. Barnett, C. L. Cleveland, *Phys. Rev. B* **37**, 4637 (1988); *ibid.*, p. 4647.
5. See review by U. Landman and W. D. Luedtke, *Appl. Surf. Sci.* **60/61**, 1 (1992), and other articles therein.
6. For recent simulations of the dynamics of energetic collisions between atomic clusters and solid surfaces, see C. L. Cleveland and U. Landman, *Science* **257**, 355 (1992).
7. For recent experiments of molecular beam scattering of rare gas atoms from liquid surfaces, see M. E. Saecker, S. T. Govoni, D. V. Kowalski, M. E. King, G. M. Nathanson, *Science* **252**, 1421 (1991).
8. For experiments of cluster-solid surface collisions, see U. Even, P. de Lange, H. Jonkman, J. Kommandeur, *Phys. Rev. Lett.* **56**, (1986); R. J. Beuhler, G. Friedlander, L. Friedman, *ibid.* **63**, 1292 (1989); R. D. Beck, P. St. John, M. L. Homer, R. L. Whetten, *Science* **253**, 879 (1991); P. St. John, R. D. Beck, R. L. Whetten, *Phys. Rev. Lett.* **69**, 1467 (1992).
9. T. P. Martin, *Phys. Rep.* **95**, 167 (1983); see also J. Luo, U. Landman, J. Jortner, in *Physics and Chemistry of Small Clusters*, P. Jena, B. K. Rao, S. N. Khanna, Eds. (Plenum, New York, 1987), p. 201.
10. C. R. A. Catlow, K. M. Diller, M. J. Norgett, *J. Phys. C* **10**, 1395 (1977); in our calculations, the effective second-neighbor $1/r^6$ term in the interionic interaction potentials was neglected.
11. G. C. Maitland, M. Rigby, E. B. Smith, W. A. Wakeham, *Intermolecular Forces* (Clarendon, Oxford, United Kingdom, 1981).
12. R. Ahrlichs, H. J. Bohm, S. Brode, K. T. Tang, J. P. Toennies, *J. Chem. Phys.* **88**, 6290 (1988).
13. J. R. Fox and H. C. Andersen, *J. Phys. Chem.* **88**, 4019 (1989).
14. M. P. Allen and D. J. Tildesley, *Computer Simulations of Liquids* (Clarendon, Oxford, United Kingdom, 1987).
15. For a complete discussion, see H.-P. Cheng and U. Landman (in preparation). The dependence of the energy transfer efficiency on the effective mass ratio between the collision partners studied in the context of atom-surface collisions and accommodation, within the framework of binary collisions, is not applicable in our case. See F. O. Goodman and H. Wachman, *Dynamics of Gas-Surface Scattering*, (Academic Press, New York, 1976); A. Amirav, M. J. Cardillo, P. L. Trevor, C.

- Lim, J. C. Tully, *J. Chem. Phys.* **87**, 1796 (1987); S. R. Cohen, R. Naaman, J. Sagiv, *Phys. Rev. Lett.* **58**, 1208 (1987), and (7).
16. The dependence of the probability of occurrence of glassy structures on the initial temperature and quench rate of the melt are well known. For clusters, such dependencies have been investigated in a recent computer simulation study by J. P. Rose and R. S. Berry [*J. Chem. Phys.* **98**, 3262 (1993)]. Furthermore, the inhibition of transformations of high-energy structural isomers to the ground-state structure at temperatures below a characteristic transition temperature has been discussed in the context of reactive cluster collisions in H.-P. Kaukonen, U. Landman, C. L. Cleveland, *J. Chem. Phys.* **95**, 4997 (1991).
 17. K. S. Suslick, *Science* **247**, 1439 (1990).
 18. A. P. Baikov, B. A. Ivanchenko, V. I. Motorin, S. L.

- Musher, A. F. Shester, *Phys. Lett. A* **113**, 38 (1985); C. J. Lin, F. Spaepen, D. Turnbull, *J. Non-Cryst. Solids* **61/62**, 767 (1984); P. Mazzoldi *et al.*, *Phys. Rev. Lett.* **44**, 88 (1980); H. A. Davis and G. B. Hull, *J. Mater. Sci.* **11**, 215 (1987).
19. We acknowledge assistance by C. L. Cleveland, in particular his help in generating Fig. 3. We thank J. R. Stevenson for bringing the work in (18) to our attention and J. P. Rose and R. S. Berry for sending a preprint of their work (16) before publication. Supported by U.S. Department of Energy (DOE) grant FG05-86ER-45234. Calculations performed at the National Energy Research Supercomputer Center, Livermore, CA, and at the Florida State Supercomputer Center through computer time grants from the DOE.

17 December 1992; accepted 23 March 1993

A Strategy for the Solid-Phase Synthesis of Oligosaccharides

Samuel J. Danishefsky,* Kim F. McClure, John T. Randolph, Roger B. Ruggeri

Repeating glycosidic linkages of oligosaccharides can be synthesized by solid-phase methods. Glycals were attached to a polystyrene copolymer with a silyl ether bond and were activated to function as glycosyl donors with 3,3-dimethyldioxirane. Glycosidation was performed by reactions with a solution-based acceptor (itself a glycal). Excess acceptor and promoter were removed by rinsing after each coupling, and the desired oligosaccharides were then easily obtained from the polymer by the addition of tetra-*n*-butylammonium fluoride. By this method, glycosidations are stereospecific and interior deletions are avoided.

Of the three major classes of biopolymers, the synthesis of polysaccharides has proven to be the most difficult. In the assembly of polypeptides and poly(2-desoxynucleotides), selection is not a problem as there is no stereochemistry in the repeating bond constructions (amide and phosphate, respectively). In contrast, each glycosidic bond to be fashioned in a growing oligosaccharide constitutes a new locus of stereogenicity and possible complexity (Fig. 1).

Furthermore, the problem of differential protection of potentially competing functions is rather formidable in the case of oligosaccharides. For instance, the extension of an oligosaccharide at either its "reducing" or "nonreducing" end by a single glucose entity requires the identification of one of five hydroxyls of the glucose to function as the glycosyl donor or acceptor, respectively (Fig. 2). In peptide bond formation, on the other hand, one need ordinarily be concerned with a single amino group (acyl acceptor) and a single carboxyl function (acyl donor) or, less commonly, two such moieties per unit (compare with lysine and aspartic acid) (1). In the synthesis of oligomers of 2-desoxynucleotides, one of two grossly different hydroxyl groups

must be distinguished, per molecule, for each elongation (2).

Synthesis of structurally defined oligopeptides and oligonucleotides has benefited greatly from the feasibility of conducting such processes on various polymer supports. The anchoring of one component to an insoluble support allows, in principle, the use of a large excess of the coupling partner (as well as promoter reagents) while keeping the final purification problem manageable. Thus, limiting yields are improved by mass action. In some cases, such syntheses can be engineered for nearly automated execution. In contrast, the overwhelming majority of carbohydrate constructions are still conduct-

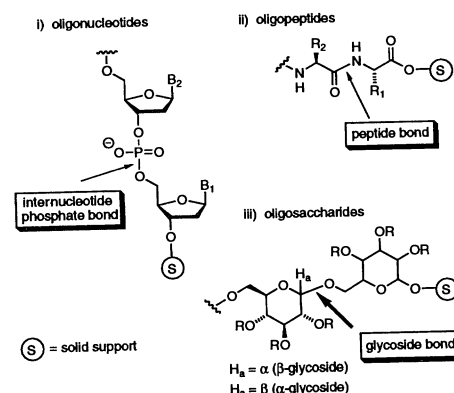


Fig. 1. Solid-phase synthesis of biopolymers.

Department of Chemistry, Yale University, New Haven, CT 06511.

*To whom correspondence should be addressed.